The Astrophysical Journal, 956:21 (9pp), 2023 October 10 https://doi.org/10.3847/1538-4357/acf37c
© 2023. The Author(s). Published by the American Astronomical Society.
OPEN ACCESS

An Optically Discovered Outburst from XTE J1859+226

Eric C. Bellm[1], Yuankun Wang[1], Jan van Roestel[2], Rebecca A. Phillipson[3], Michael W. Coughlin[4], John A. Tomsick[5], Steven L. Groom[6], Brian Healy[7], Josiah Purdum[8], Ben Rusholme[6], Jesper Sollerman[9], Peter Bealo[10], Stefano Lora[10,11], Eddy Muyllaert[10], Ivo Peretto[10,11], and Erik J. Schwendeman[10]
[1] DIRAC Institute, Department of Astronomy, University of Washington, 3910 15th Avenue NE, Seattle, WA 98195, USA; ecbellm@uw.edu
[2] Anton Pannekoek Institute for Astronomy, University of Amsterdam, 1090 GE Amsterdam, The Netherlands
[3] Villanova University, Department of Physics, Villanova, PA 19085, USA
[4] School of Physics and Astronomy, University of Minnesota, Minneapolis, MN 55455, USA
[5] Space Sciences Laboratory, 7 Gauss Way, University of California, Berkeley, CA 94720-7450, USA
[6] IPAC, California Institute of Technology, 1200 E. California Boulevard, Pasadena, CA 91125, USA
[7] School of Physics and Astronomy, University of Minnesota, 116 Church Sreet SE, Minneapolis, MN 55455, USA
[8] Caltech Optical Observatories, California Institute of Technology, 1200 E. California Boulevard, Pasadena, CA 91125, USA
[9] Department of Astronomy, The Oskar Klein Center, Stockholm University, AlbaNova, SE-10691 Stockholm, Sweden
[10] American Association of Variable Star Observers, 185 Alewife Brook Parkway, Suite 410, Cambridge, MA 02138, USA
[11] Marana Space Explorer Center, Pasquali Road, Marana Di Crespadoro, Vicenza, I-36070, Italy
Received 2023 May 18; revised 2023 July 26; accepted 2023 August 21; published 2023 October 4

Abstract

Using the Zwicky Transient Facility, in 2021 February we identified the first known outburst of the black hole X-ray transient XTE J1859+226 since its discovery in 1999. The outburst was visible at X-ray, UV, and optical wavelengths for less than 20 days, substantially shorter than its full outburst of 320 days in 1999, and the observed peak luminosity was 2 orders of magnitude lower. Its peak bolometric luminosity was only 2×10^{35} erg s^{-1}, implying an Eddington fraction of about 3×10^{-4}. The source remained in the hard spectral state throughout the outburst. From optical spectroscopy measurements we estimate an outer disk radius of 10^{11} cm. The low observed X-ray luminosity is not sufficient to irradiate the entire disk, but we observe a surprising exponential decline in the X-ray light curve. These observations highlight the potential of optical and infrared synoptic surveys to discover low-luminosity activity from X-ray transients.

Unified Astronomy Thesaurus concepts: Low-mass x-ray binary stars (939); X-ray binary stars (1811)

Supporting material: data behind figure

1. Introduction

Transient black hole X-ray binaries (XRBs) exhibit large outbursts driven by instabilities in their accretion disks. Canonical outbursts transition through a sequence of states of differing intensity, spectral hardness, and variability bracketed by a hard, low-luminosity state near quiescence and a soft state at peak outburst flux (e.g., Remillard & McClintock 2006; Kalemci et al. 2022). These states reflect the changing conditions of the accretion disk, corona, and jet as the outburst progresses. This evolution is broadly understood in the context of the disk instability model (for a review, see Hameury 2020), in which increased densities cause the disk temperature to rise locally, ionizing hydrogen and creating a viscous instability that propagates through the disk and increases the mass transfer onto the compact object. In XRBs, irradiation of the disk by the compact object prolongs their outbursts and increases their recurrence times relative to dwarf novae (e.g., King & Ritter 1998). However, the exact drivers of the state transitions are still not understood in detail.

Some outbursts do not exhibit the full range of spectral states: such "failed-transition" or "hard-only" outbursts brighten without reaching the soft state (e.g., Alabarta et al. 2021, and references therein). Almost 40% of outbursts fail to transition, and individual binaries can exhibit both full and failed outbursts (Tetarenko et al. 2016). Different mass accretion rates may influence whether state transitions occur. Alabarta et al. (2021) noted that in GX 339−4, the quiescent optical and infrared (O/IR) flux levels were higher prior to failed-transition outbursts than prior to successful ones.

Further observations of failed-transition outbursts can help pinpoint their causes. As failed-transition outbursts are less luminous than canonical outbursts, they are more difficult to discover with all-sky X-ray monitors. Due to their faintness, some may fall in the phenomenological class of low-luminosity ($L_X \sim 10^{34}$–10^{36} erg s^{-1}) very faint x-ray transients (VFXTs; Wijnands et al. 2006; Heinke et al. 2015), which may include outbursts from short-period accreting systems with intrinsically small accretion disks as well as failed-transition outbursts from portions of larger disks. VFXTs are typically discovered through deep, cadenced observing programs by narrow-field X-ray telescopes (e.g., Swank & Markwardt 2001; Kuulkers et al. 2007; Bahramian et al. 2021), and so must sacrifice areal coverage for sensitivity. Alternatively, optical and infrared observations by synoptic surveys or dedicated monitoring programs (e.g., Zhang et al. 2019; Saikia et al. 2023) can also remove the selection effect imposed by X-ray monitor detection and provide a more comprehensive view of black hole accretion.

XTE J1859+226 was first discovered in outburst at 250 mCrab in 1999 by the All-Sky Monitor on the Rossi X-ray Timing Explorer (Wood et al. 1999) and peaked at 1.5 Crab 8 days later (Focke et al. 2000). Follow-up observations revealed a 15th magnitude optical counterpart with broad

Original content from this work may be used under the terms of the Creative Commons Attribution 4.0 licence. Any further distribution of this work must maintain attribution to the author(s) and the title of the work, journal citation and DOI.

Balmer and He II emission lines (Garnavich et al. 1999; Wagner et al. 1999). A radio counterpart with flux ∼10 mJy was also detected (Pooley & Hjellming 1999). X-ray observations revealed a hard power-law spectrum with an evolving quasi-periodic oscillation (dal Fiume et al. 1999; Markwardt et al. 1999). In combination, these features suggested the discovery of a new black hole X-ray transient.

In total the 1999 outburst lasted for about 320 days, with several late-time reflares peaking around $m_R \sim 15$ mag, before returning to a quiescent magnitude of $m_R \sim 22.5$ (e.g., Zurita et al. 2002). The initial hard-state behavior of the outburst during the rise to a high-luminosity soft state provoked a recognition that this behavior is common among XRBs (Brocksopp et al. 2002). Tomsick et al. (2003) reported Chandra X-ray observations of XTE J1859+226 in quiescence; its faint spectrum was consistent with an absorbed power law with a 0.3–8 keV luminosity of 2.2×10^{31} $(d/8\ \mathrm{kpc})^2$ erg s^{-1}. Radial velocity observations by Filippenko & Chornock (2001) suggested the presence of a very massive black hole (BH); however, later observations by Corral-Santana et al. (2011) provided a revised orbital period of 6.58 hr, a mass function of $4.5 \pm 0.6\ M_\odot$, and a lower limit mass of $M_{\rm BH} > 5.42\ M_\odot$ with inclination $i < 70°$. As discussed in Tetarenko et al. (2016), distance estimates in the literature for this source are sensitive to changing assumptions of the orbital period and secondary spectral type. They adopt a fiducial distance estimate of 8 ± 3 kpc taken from Hynes (2005). We will use the same value in this paper, although we note that the shorter orbital period and later spectral type proposed by Corral-Santana et al. (2011) lead to model fits at a greater distance of ∼14 kpc.

Corral-Santana et al. (2010) reported that in 2010 August XTE J1859+226 had rebrightened by ∼1 mag in the optical and showed short-timescale flaring. This brightening was not accompanied by an increase in the X-ray flux.

In 2021 February we identified a larger optical brightening (Bellm 2021a) of XTE J1859+226 to $m_r \sim 18.9$ mag using the Zwicky Transient Facility (ZTF; Bellm et al. 2019b; Graham et al. 2019). This was accompanied by an X-ray brightening to a 0.3–10 keV flux of $7.9^{+2.0}_{-1.5} \times 10^{-12}$ erg cm^{-2} s^{-1} (Bellm 2021b). However, continued monitoring by these facilities over the subsequent weeks saw the source flux peak and decline by 1.5 mag. This decline was also reported by the XB-NEWS project (Caruso et al. 2021). Despite its low luminosity and short duration, in the taxonomy of Zhang et al. (2019), the 2021 outburst is classified as a new outburst since the time elapsed since the full 1999 outburst is much greater than the duration of the 1999 outburst.

In Section 2 we describe the discovery and observations of the outburst. We analyze these observations in Section 3. We conclude in Section 4 with implications for future observations of low-luminosity outbursts.

2. Observations

2.1. Discovery of the Outburst

The Zwicky Transient Facility (Bellm et al. 2019b; Graham et al. 2019) uses a large mosaic camera (Dekany et al. 2020) to survey the Northern Hemisphere sky ($\delta > -30°$) in three optical bands (g, r, and i) to typical depths of 20.5 mag with a cadence of two nights or faster (Bellm et al. 2019a). Near-real-time difference imaging pipelines (Masci et al. 2019) identify transients, variables, and moving objects. Motivated by a desire to identify compact binary outbursts and state changes (see also Russell et al. 2019), we are monitoring the public alert stream (Patterson et al. 2019) for a watchlist of known X-ray binaries using ANTARES (Matheson et al. 2021).

On 2021 February 4 ZTF observed a field containing XTE J1859+226 five times in the r band as part of its public twilight survey. We received a notification from the ANTARES system of a new source, internally designated ZTF21aagyzqr, coincident with XTE J1859+226.[12] The ZTF detections were at $m_r \sim 18.9$ mag, substantially brighter than the quiescent magnitude of $m_R \sim 22.5$ (Zurita et al. 2002). We issued a circular (Bellm 2021a) encouraging further observations in anticipation of additional brightening. We also triggered Swift target-of-opportunity observations and confirmed that the X-ray flux had increased by three orders of magnitude relative to the quiescent level (Bellm 2021b). We used a customized Skyportal (van der Walt et al. 2019; Coughlin et al. 2023) instance ("Fritz") for managing follow-up data.

2.2. Optical Observations

2.2.1. Photometry

We obtained point-spread function forced photometry measurements on ZTF difference images (Masci et al. 2019). We corrected the resulting differential photometry for the flux of the counterpart in the reference image, which is detected at $m_r \sim 21.7$ mag in the r-band ZTF reference image. The image is uncrowded in both the direct and difference images; the nearest PanSTARRS1 source is 1.″8 away and subtracts cleanly. We excluded observations with `procstatus` values other than 0 or 57 to avoid biased photometry. This returned more than 1400 forced flux measurements beginning in 2018 March. Most were consistent with nondetections, but 214 were detections with signal-to-noise ratio (S/N) greater than 3. Of these detections, 124 were taken in a period of intensive monitoring on 2018 August 7–8. The median 5σ upper limit was 20.9 mag in the g band and 20.5 mag in the r band.

We obtained difference-image forced photometry from the ATLAS forced photometry service (Tonry et al. 2018). We required reduced $\chi^2 < 20$, `err` $= 0$, and magnitudes greater than 10 to reject clearly spurious measurements. This yielded 1606 forced flux measurements beginning in 2015 October, of which 56 were detections with S/N > 3. The median 5σ upper limit was 19.2 mag.

We imaged XTE J1859+226 in Sloan Digital Sky Survey g, r, and i bands with the Rainbow Camera of the Spectral Energy Distribution Machine (SEDM; Blagorodnova et al. 2018) on the Palomar 60 inch telescope (P60) on 2021 February 8. Automated reductions were performed using the methods described in Fremling et al. (2016) and Blagorodnova et al. (2018).

In anticipation of further brightening of the source, we sent an Alert Notice[13] to the American Association of Variable Star Observers (AAVSO). We retrieved the resulting photometry from the online download portal (Kloppenborg 2022).

2.2.2. Spectroscopy

Along with three-color photometry, on 2021 February 8 we obtained a low-resolution spectrum of XTE J1859+226 using

[12] The ANTARES page for this object can be found at https://antares.noirlab.edu/loci/ANT2021dn4jk.

[13] #729; https://www.aavso.org/aavso-alert-notice-729.

Table 1
Swift Observations Used in This Work

Obsid	Start Time (MJD)	XRT Exposure (s)	UVOT Filter
00031827002	59,251.97437910605	1990	*V*
00031827003	59,252.89778221208	991	*V*
00031827004	59,255.55894562874	847	*UVW1*
00031827005	59,259.73500215374	934	*UVW1*
00031827006	59,261.65729843129	869	*UVW2*
00031827007	59,261.98584341670	742	*V*
00031827009	59,263.64414707874	864	*V*
00031827010	59,265.23678571347	899	*V*
00031827011	59,266.16805541601	719	*UVM2*
00031827012	59,267.75982711509	1009	*V*
00031827013	59,273.22360766786	914	*UVW2*

the P60 SEDM (Blagorodnova et al. 2018). The on-source exposure time was 2700 s. Automated reductions were performed using `pysedm` (Rigault et al. 2019; Kim et al. 2022).

We obtained a long-slit spectrum of XTE J1859+226 using the Low-Resolution Imaging Spectrometer (LRIS; Oke et al. 1995) on Keck I on 2021 February 15. The instrument was configured with a 1.″5 wide slit, the 560 dichroic, the 400/3400 grism, and the 400/8500 grating with a central wavelength of 7828 Å. The blue-side exposure time was 500 s and the red-side exposure time was 800 s. We reduced the data using `LPipe` (Perley 2019).

2.3. X-Ray Observations

We obtained a series of Swift observations between 2021 February 6 and 28 (Table 1). We used the Swift X-Ray Telescope (XRT) data products generator[14] (Evans et al. 2007, 2009) to produce count rates, hardness ratios, and spectra for each observation. Due to low count rates we grouped observations 00031827006, 00031827007, and 00031827009 into a single summed spectrum. After fitting a spectral model to this summed spectrum, we froze the spectral parameters and fit the flux normalization in each constituent spectrum. Observations 00031827010, 00031827011, 00031827012, and 00031827013 had too few counts to produce spectra.

NuSTAR observed XTE J1859+226 for 40.4 ks on 2021 February 13. We obtained publicly available NuSTAR observations (obsid 90701305002, P.I. Harrison; see also Draghis et al. 2021, 2023) from the HEASARC and processed them using standard procedures with `nuproducts` under Heasoft v6.28. We extracted spectra for each module using circular apertures of 40″ radius at the position of XTE J1859+226 and extracted background spectra from circular apertures of 115″ radius placed on the same chip.

We performed spectral fits using ISIS (Houck & Denicola 2000). We fit the Swift-XRT data from 0.3 to 10 keV and NuSTAR data from 3 to 30 keV. We used the `tbabs` absorption model with `vern` cross sections (Verner et al. 1996) and `wilm` abundances (Wilms et al. 2000). We rebinned the spectra using the binning scheme of Kaastra & Bleeker (2016) and required a minimum of three counts per bin. We fit using the `wstat` fit statistic (Wachter et al. 1979; Arnaud 2000), which provides a maximum likelihood parameter estimate in the case of low-count Poisson-distributed source and background data. We report uncertainties on the best-fit parameters at the 1σ confidence level.

We also retrieved publicly available daily count rates for XTE J1859+226 from MAXI (Matsuoka et al. 2009) and Swift's Burst Alert Telescope (BAT; Krimm et al. 2013).

2.4. UV Observations

We reduced the UVOT data for the Swift observations described in Section 2.3 using standard procedures with `uvotsource` under Heasoft v6.28. We used the standard circular source extraction region of 5″ radius and placed a circular background region of 12″ radius nearby. No contaminating sources were apparent in the images. We report source measurements with S/N greater than 3; when undetected we provide 5σ upper limits.

3. Analysis

3.1. Outburst Duration

Figure 1 presents the optical and X-ray photometry of the outburst. Because XTE J1859+226 was emerging from behind the Sun, we do not have strong constraints on the onset of the outburst. The last ZTF nondetection was on 2020 December 21 (Section 3.2). While we reported in Bellm (2021a) that ZTF had not detected XTE J1859+226 one night prior to the onset of the outburst, those observations were in a different, overlapping field and the position of XTE J1859+226 fell in a chip gap. The upper limits included in the ZTF alert were estimates over the CCD rather than forced photometry at the source position. Accordingly the ZTF observations on 2021 February 3 do not provide information on the state of XTE J1859+226 at that time.

Our Swift-XRT observations did not capture the rising phase of the outburst—the peak flux was observed in the first XRT observation 59 hr after the first ZTF detection. In many cases the optical outburst is expected to precede an X-ray brightening (Russell et al. 2019), so it is plausible that our first Swift observations are near the peak of the outburst in the X-ray region. Nevertheless, reflares and other temporal irregularities are common in XRB outbursts. We searched other instruments for observations that might constrain the behavior of the system prior to the first ZTF detection on 2021 February 4. In the optical, ZTF's last nondetection on 2020 December 21 was more constraining than those of XB-NEWS (2020 November 16; Caruso et al. 2021) and ATLAS (2020 December 4).

In the X-ray band, no excess above an S/N of 3 is visible in the MAXI daily count rate up to 2021 January 3 or on or after 2021 January 28; the 5σ flux limit is 0.087 photons $\mathrm{cm^{-2}\,s^{-1}} = 5.7\times10^{-9}$ erg $\mathrm{cm^{-2}\,s^{-1}}$ (2–20 keV) = 0.23 Crab under MAXI's assumption of a Crab spectrum. Similarly, Swift-BAT observations rule out X-ray emission at 5σ flux levels of 0.0075 counts $\mathrm{cm^{-2}\,s^{-1}}$ (15–50 keV) up to 2021 January 27 or starting on 2021 February 3. Assuming a $\Gamma = 2$ power law with $n_{\mathrm{H}} = 3.1\times10^{21}$ atoms $\mathrm{cm^{-2}}$ (Section 3.4), the Swift-BAT count rate limit corresponds to a 15–50 keV energy flux limit of 2.7×10^{-9} erg $\mathrm{cm^{-2}\,s^{-1}} = 0.15$ Crab. The BAT limit is thus more constraining in both flux and time. Given the brevity of the gap in BAT coverage relative to major XRB outbursts (Tetarenko et al. 2016) as well as the observed outburst duration, we consider it unlikely that an outburst above the BAT threshold was missed due to the short period of Sun constraint. We can therefore rule out X-ray luminosities brighter

[14] https://www.swift.ac.uk/user_objects/

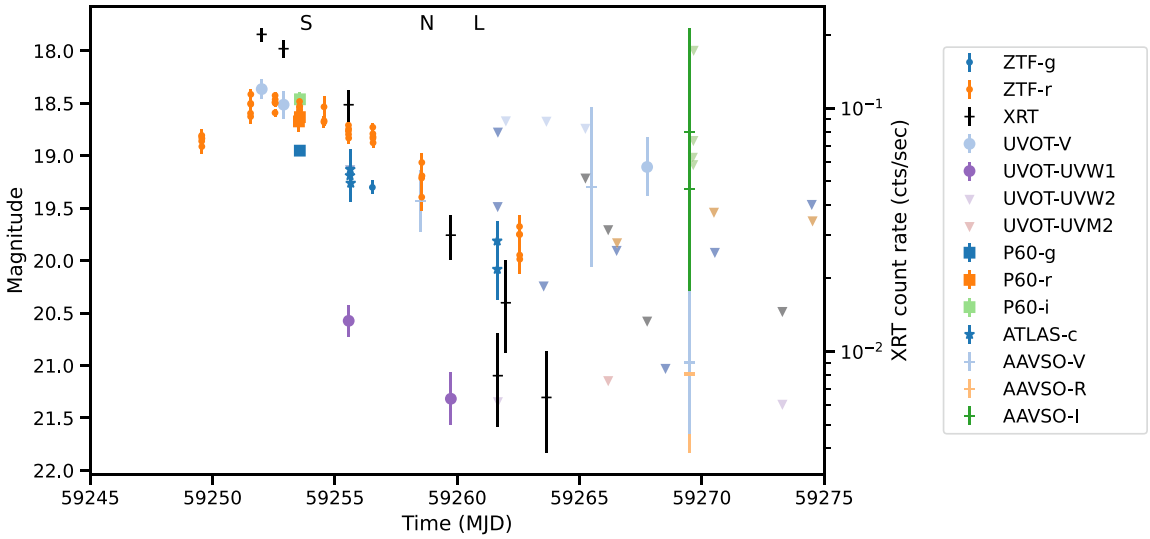

Figure 1. Outburst light curve for XTE J1859+226 from ZTF, P60, AAVSO, and Swift-UVOT and XRT. Detections (S/N > 3) are marked with points; 5σ upper limits are denoted with triangles. Text labels indicate the times of SEDM spectroscopy (S), NuSTAR observations (N), and Keck-LRIS spectroscopy (L).
(The data used to create this figure are available.)

than $4 \times 10^{37}(d/8\,\mathrm{kpc})^2\,\mathrm{erg\,s^{-1}}$ (MAXI) and $2 \times 10^{37}(d/8\,\mathrm{kpc})^2\,\mathrm{erg\,s^{-1}}$ (BAT) during these intervals. While these limits are 2 orders of magnitude higher than the observed Swift-XRT X-ray flux (Section 3.4), they still exclude outbursts brighter than 10% of the peak flux of the 1999 outburst.

There is weak evidence for rebrightening or variability at late times in the outburst in the UVOT *V* band as well as in several AAVSO measurements, although ZTF places some deeper nondetection limits during comparable time periods.

Despite the lack of strong constraints on the time of onset of the outburst, we can coarsely estimate the overall duration of the outburst if we assume no prior activity. The time between the first ZTF *r*-band detection and the first nondetection is 16.9 days; however, there was a four-night gap due to bad weather between the last ZTF detection and the first nondetection. In Swift-XRT the same calculation yields 13.2 days, although 2.5 days elapsed between the first ZTF detection and the first XRT observation. Most classical XRB outbursts show a temporal profile with a fast rise and exponential decay. If we assume the first XRT observation is the peak of the outburst, we can estimate a likely upper limit for the outburst duration by doubling the X-ray decay time. Taking these measurements together, we estimate a plausible range of durations for this outburst at ∼16–26 days, although we cannot rule out a duration of 60 days if optical activity began immediately after the last ZTF observation in 2020 December. This duration is much shorter than normal outbursts from black hole low-mass X-ray binaries, which typically last hundreds of days. Less than 3% of the outbursts cataloged in Tetarenko et al. (2016) had durations less than 30 days, and 7% had durations less than 60 days. However, faint X-ray transients such as this one tend to have shorter durations (Heinke et al. 2015, and references therein).

3.2. Quiescent Light Curve

Figure 2 shows the ZTF forced photometry light curve of XTE J1859+226 in quiescence from 2018 March to 2023 February. There is clear evidence of short-timescale variability, with irregular single-epoch detections at 21.0–21.5 mag in the *r* band. However, averaging these measurements on timescales of 100 days suggests a fairly stable average quiescent level of $m_r \sim 21.9$ mag prior to the outburst. XTE J1859+226 is undetected even in bins of 100 days in the *g* band, with 5σ limits reaching $m_g \gtrsim 23.0$ mag.

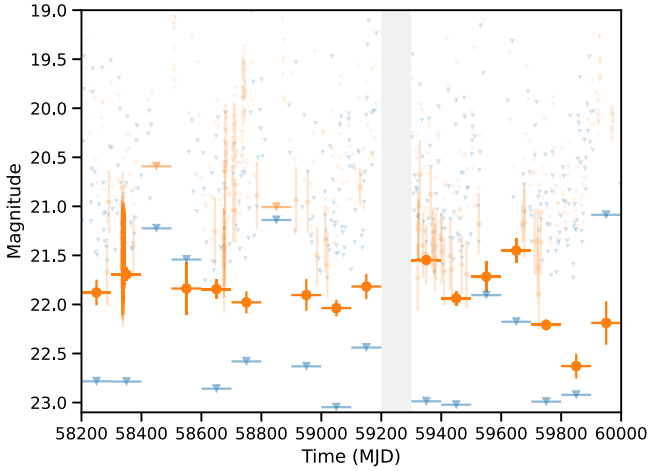

Figure 2. ZTF forced photometry light curve of XTE J1859+226 in quiescence in *g* (blue) and *r* (orange) bands. We plot both single-epoch measurements (points) and error-weighted coadditions over 100 days (points with horizontal error bars). Detections with S/N greater than 3 are marked with circles, and 5σ upper limits with triangles. We exclude the outburst interval (gray region).

The ZTF data indicate that for at least 1000 days before and 400 days after the outburst, XTE J1859+226 was about 3/4 of a magnitude brighter in the *r* band than its deepest quiescent level. Around MJD 59,800, the source faded to $m_r \sim 22.5$ mag, near the quiescent level reported by Zurita et al. (2002). From a detailed study of GX 339−4, Alabarta et al. (2021) suggested that brighter O/IR emission was predictive of a failed-transition outburst, which is consistent with these observations.

However, the elevated O/IR flux levels after the outburst and the delayed fading to true quiescence appear more difficult to explain in this framework.

We also investigated the ATLAS long-term light curve. Because the ATLAS data have a similar number of epochs over a longer baseline but are more than one magnitude shallower than ZTF, we did not coadd them. The ATLAS data exhibit several high-amplitude detections, including 10 data points brighter than 18.5 mag. In all cases other than the outburst reported here, however, these detections do not form a coherent outburst temporal profile—deeper upper limits are interspersed. These imply either fast variability on timescales of hours to days or imaging artifacts. We examined the cutout images for these differences and found that all reported detections brighter than 18.5 mag were due to imaging artifacts such as open-shutter readout, elevated sky backgrounds, and image differencing failures. Accordingly, we do not find evidence in the ATLAS data for other outbursts since 2015 October.

3.3. Spectral Energy Distribution

As seen in Figure 1, we have few epochs with simultaneous multiwavelength coverage, making it difficult to distinguish the shape of the spectral energy distribution (SED) from intrinsic variability. As a point estimate, we took the P60 *g*-, *r*-, and *i*-band measurements obtained near the optical peak. We dereddened these using a Fitzpatrick (1999) extinction law implemented in the Python package `dust_extinction` with $R_V = 3.1$ and $E(B-V) = 0.58$ mag as reported in Hynes (2005). Fitting these with a blackbody using least squares, we obtain a temperature estimate of $18{,}000 \pm 1500$ K. As at this phase the outburst is substantially brighter than the quiescent state of the system we can be confident that the SED is dominated by the disk. Notably, this temperature is comfortably above the temperature of 10^4 K needed to ionize hydrogen, distinguishing this failed-transition outburst from the "misfired outburst" of Cen X-4 reported by Baglio et al. (2022).

3.4. X-Ray Spectra

Figure 3 shows the Swift-XRT hardness–intensity diagram. The X-ray hardness remains roughly constant as the outburst dims, remaining in a hard state throughout the observations.

We performed detailed spectral fits to the epochal Swift data as well as joint fits of NuSTAR data and Swift epoch 00031827005. The data are well fit by an absorbed power law (`tbabs × powerlaw`) in all epochs. The power law is best constrained in the joint Swift–NuSTAR epoch (Figure 4), with $\Gamma = 1.9 \pm 0.1$ and wstat = 129.4 for 124 degrees of freedom. A `tbabs × diskbb` model provided a substantially worse fit, with wstat = 164.9 for 124 degrees of freedom and more systematic residuals. We froze the column density of neutral hydrogen to its best-fit value of $3.1^{+1.0}_{-0.7} \times 10^{21}$ atoms cm^{-2} from the first Swift epoch, as the value was more poorly constrained in the fainter later epochs. This column density is comparable to the values reported by Farinelli et al. (2013) during the 1999 outburst as well as the total Galactic line-of-sight value[15] of 3.5×10^{21} atoms cm^{-2} (Willingale et al. 2013). The best-fit power law is consistent within errors with a constant value at all epochs (Figure 5), in line with the lack of evolution seen in the hardness–intensity diagram (Figure 3).

[15] https://www.swift.ac.uk/analysis/nhtot/index.php

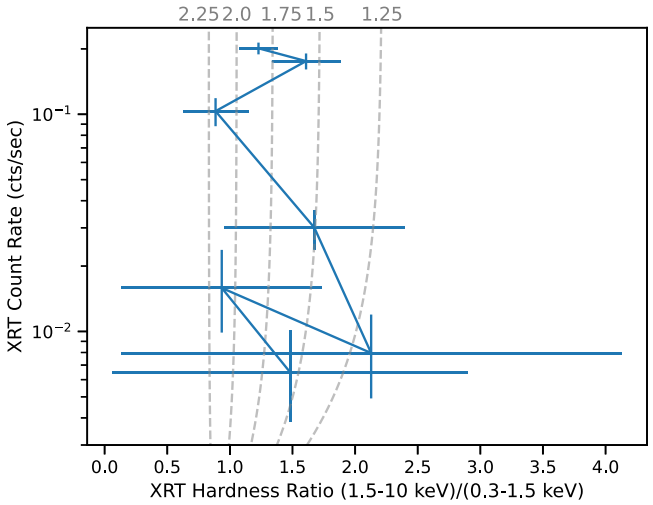

Figure 3. Swift-XRT hardness–intensity diagram. Lines connect consecutive measurements; the earliest measurements are the brightest (see Figure 1). Dashed lines show the hardness–intensity values produced by absorbed power-law spectra with $n_{\rm H} = 3.1 \times 10^{21}$ atoms cm^{-2} and spectral indices Γ from 1.25 to 2.25 (top labels).

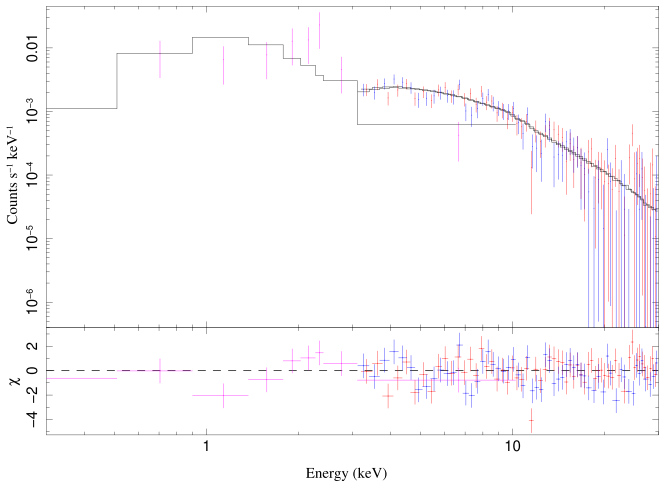

Figure 4. Absorbed power-law fit to Swift and NuSTAR spectra.

While some residual structure is apparent, we did not find strong evidence for the marginal 6.7 and 8.4 keV emission lines reported by Draghis et al. (2021). As in their analysis, fits with an additional Gaussian emission line forced near these positions yielded confidence intervals for the line FWHM consistent with zero for the additional components and only modest changes in the fit statistic.

If we assume the first Swift epoch corresponds to the maximum brightness of the outburst, we estimate a peak bolometric flux of $2.6^{+0.7}_{-0.4} \times 10^{-11}$ erg cm^{-2} s^{-1}. This implies a peak bolometric luminosity of $L \approx 2.0^{+0.5}_{-0.3} \times 10^{35} (d/8\ {\rm kpc})^2$ erg s^{-1}. The Eddington fraction at peak is thus $2.8^{+0.7}_{-0.4} \times 10^{-4} (d/8\ {\rm kpc})^2 (M_{\rm BH}/5.4\ M_\odot)^{-1}$.

3.5. Optical Spectra

Figure 6 shows the optical spectra of XTE J1859+226 at two epochs indicated by letters on the outburst light curve in Figure 1. The low-resolution SEDM spectrum taken near the outburst peak is noisy, with a blue continuum. The late-time LRIS

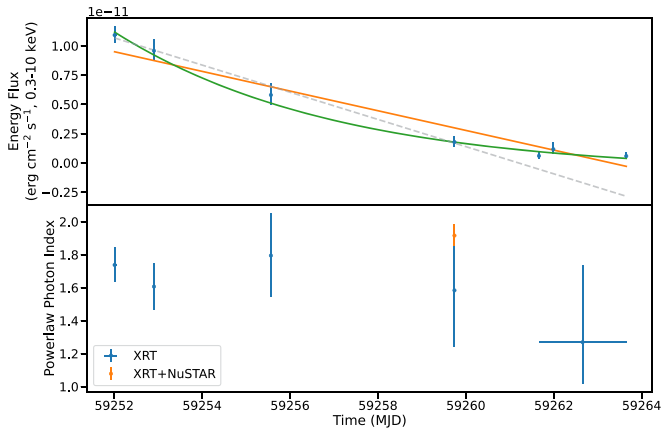

Figure 5. Time evolution of absorbed power-law parameters from spectral fits to Swift (blue) and joint Swift–NuSTAR (orange) data. Top panel: 0.3–10 keV energy flux in erg cm^{-2} s^{-1}. The best-fit exponential (green), linear (orange), and limited-range linear (gray dashed) models are overplotted. Bottom panel: best-fit spectral index Γ, where $F(E) \propto E^{-\Gamma}$.

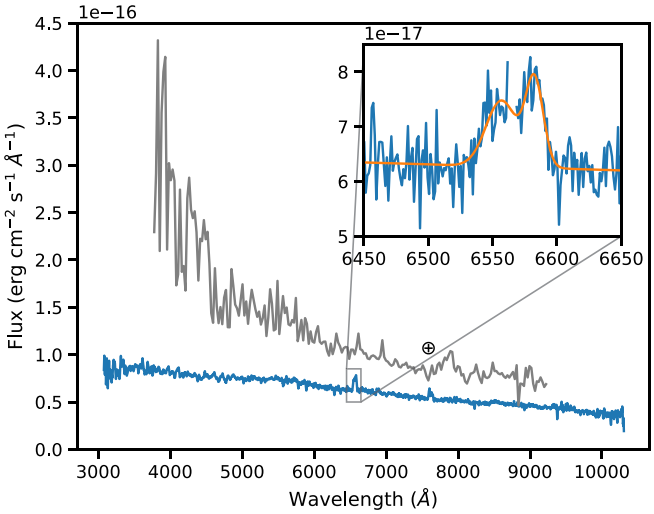

Figure 6. Optical spectra (gray: SEDM; blue: LRIS) of XTE J1859+226 in outburst. The full LRIS spectrum is convolved with an 8 pixel boxcar filter for plot clarity. Inset: double Gaussian fit (orange) to the LRIS Hα emission line. The gap in the data corresponds to the pixels excluded due to contamination by a cosmic ray.

spectrum exhibits broadened Hα emission as well as interstellar absorption lines. No other strong emission lines are present.

We fit single and double Gaussian models to the continuum-subtracted Hα line in the late-time LRIS spectrum using `pyspeckit` (Ginsburg & Mirocha 2011; Ginsburg et al. 2022). The peak of the Hα line was unfortunately contaminated by a cosmic ray; we excluded the affected pixels. The missing data make it difficult to clearly identify the morphology of the line profile. All of the model fits (single Gaussian, double Gaussian, double Gaussian with tied amplitudes and widths) were formally statistically acceptable. Noting the asymmetry in Hα in Zurita et al. (2002), we quote and plot values and bootstrap error estimates from the asymmetric two-Gaussian fit (inset, Figure 6), although the values derived from the other models are comparable. The Hα line has FWHM of 1500 ± 560 km s^{-1} and an equivalent width of 10.1 ± 0.9 Å. The two peaks are separated by 1170 ± 110 km s^{-1}.

3.6. Disk Extent

Casares (2016) interpret the peak separation DP of broad Hα emission lines as the velocity of material at the outer disk radius R_d, with $\mathrm{DP} = 2\beta\sqrt{GM/R_d}\,\sin i$. β is the fraction by which the outer disk is sub-Keplerian; Casares (2016) find a value of $\beta = 0.77$ is broadly consistent with their sample of BH XRBs. Assuming $q \lesssim 0.7\,M_\odot/5.4\,M_\odot = 0.13$ for a K4V secondary of $0.7\,M_\odot$ (Cox 2000; Corral-Santana et al. 2011), Equation (4) of Casares (2016) with $\alpha = 0.42$ and $\beta = 0.77$ would predict a ratio of $\mathrm{DP/FWHM} = 0.55$, which is consistent within the relatively large error bars of our measured ratio of $\mathrm{DP/FWHM} = 0.78 \pm 0.30$.

Since the system masses and inclinations are constant, we can interpret changes in the peak separation as changes in the outer radius of the emitting region of the disk. Zurita et al. (2002) report two such measurements during the 1999 full outburst. In a first epoch near the main outburst peak, they measure Balmer peak separations of 300–500 km s^{-1}. In a second phase near the peak of a subsequent minioutburst, they report larger Balmer peak separations of 500–700 km s^{-1}. If we take the larger of each of these values and compare them to the 2021 peak separation, they imply outer disk radius ratios of 1:0.51:0.18 for the 1999 outburst peak:1999 minioutburst:2021 outburst tail. The corresponding optical magnitudes at epochs at which the spectra were obtained are about $m_R \sim 15.8$, 18.3, and 19.5 mag, corresponding to flux ratios of 1:0.1:0.03. These are broadly consistent with a naive scaling of the disk area implied by the ratio of the outer radii (1:0.26:0.03).

Estimating the absolute outer disk radius of the 2021 outburst from the LRIS peak separation, we find

$$R_d \sim 10^{11}\,\mathrm{cm}\left(\frac{M_{\mathrm{BH}}}{5.4\,M_\odot}\right)\left(\frac{\beta}{0.77}\right)^2\left(\frac{\sin i}{\sin 70^\circ}\right)^2\left(\frac{\mathrm{DP}}{1170\ \mathrm{km\ s^{-1}}}\right)^{-2}.$$

This is near the maximum allowed disk radius, which Lasota et al. (2008) parameterize as

$$R_{\max} = 2.28 \times 10^9 f\left(\frac{M_{\mathrm{BH}}}{1\,M_\odot}\right)^{1/3}\left(\frac{P_{\mathrm{orb}}}{1\ \mathrm{minute}}\right)^{2/3}\ \mathrm{cm},$$

where

$$f = \frac{0.06}{(1+q)^{2/3}}.$$

Using the parameters of Corral-Santana et al. (2011), we find $R_{\max} \sim 1.2 \times 10^{11}$ cm. This limit conflicts with our inference of a 5 times larger outer disk radius during the 1999 outburst, suggesting the true disk radius may be a factor of a few smaller. Given the uncertainties in several of the parameters, however, the overall picture remains plausible: these data suggest that XTE J1859+226 has a large disk near its maximum allowed extent.

3.7. Decay Profile

Fully irradiated accretion disks are expected to show exponential decay profiles that transition to a linear decay as the outer disk begins cooling and then to an even steeper linear decline when no irradiation is present (King & Ritter 1998). We attempted to fit an analytic exponential-to-linear temporal profile (Tetarenko et al. 2018b) to the X-ray flux light curve.[16]

[16] The late-time XRT upper limits were not constraining so we did not include them in the temporal fits.

However, the observed data were insufficient to observe such a transition.

We also fit the data with simple exponential ($f(t) = f_0 \exp(-(t - t_{\rm break})/\tau_e) + f_1$) and linear ($f(t) = f(t_0)(1 - (t - t_0)/\tau_l)$ decays (Figure 5). The exponential model provides a better fit to the data, with $\chi^2/\nu = 2.7/3 = 0.9$ compared to $\chi^2/\nu = 24.6/5 = 4.9$ for the linear model. While it has two more free parameters, the exponential model is preferred by the Akaike information criterion (AIC; Akaike 1974), although the number of data points is too small for the asymptotic validity assumptions of the AIC to strictly hold. The best-fit decay timescales were $\tau_e = 5.0 \pm 1.4$ days and $\tau_l = 63.3 \pm 0.3$ days. The exponential decay timescale is substantially shorter than those seen in full outbursts of BH XRBs, while the linear decay timescale is comparable (Tetarenko et al. 2018a).

Following King & Ritter (1998), Shahbaz et al. (1998) identified a critical luminosity for black hole accretors $L_{\rm crit} = 1.7 \times 10^{37} (R_d/10^{11}\,{\rm cm})^2\,{\rm erg\,s^{-1}}$. Below this luminosity, the outer edge of the disk will not be irradiated and the decline in the light curve should be purely linear. Our observation of an exponential decay conflicts with this prediction: the peak luminosity of $\sim 10^{35}\,{\rm erg\,s^{-1}}$ for this outburst (Section 3.4) is two orders of magnitude smaller than the critical value, but the observed X-ray decline (Section 3.1) is not linear.

In contrast, the luminosity of the 1999 outburst peaked at $2.8 \times 10^{38} (d/8\,{\rm kpc})^2\,{\rm erg\,s^{-1}}$ (Farinelli et al. 2013), within a factor of 2 of the critical luminosity luminosity for a disk 5 times larger.

We consider several possibilities to resolve this apparent contradiction. We have assumed that our first Swift-XRT measurement corresponds to the peak of the outburst. If the outburst were already underway prior to the first Swift observations, the true peak luminosity might have been higher. However, for our fiducial distance and disk radius, the critical luminosity almost exactly matches the limits provided by Swift-BAT monitoring (Section 3.1). Thus if the peak of the outburst had exceeded the critical level, it would have been detected by BAT. Extrapolating our best-fit exponential decay model backwards, we find that the bolometric luminosity would have been above the critical level before 2021 January 16, which is ruled out by BAT observations in that interval.

Our conversion of peak flux to luminosity uses a fiducial 8 kpc distance to the source. If instead we adopt the value of 14 kpc from Corral-Santana et al. (2011), the observed luminosity is a factor of three larger, still not enough to reach the critical threshold.

Similarly, a smaller disk radius R_d would lower the luminosity required to ionize the entire disk. Both β and the inclination are poorly constrained; for a range of plausible assumed values, the disk radius could be an order of magnitude smaller. This still leaves a gap of another order of magnitude to the critical luminosity but would allow for an unseen outburst precursor below the BAT flux limits. Alternatively, our best-fit exponential decay timescale can be used to infer the disk radius, with $\tau_e = R_d^2/3\nu$ (Shahbaz et al. 1998), where ν is the unknown disk viscosity. This yields a disk radius of

$$3.6 \times 10^{10} \left(\frac{\tau_e}{5\,{\rm days}}\right)^{1/2} \left(\frac{\nu}{10^{15}\,{\rm cm^2\,s^{-1}}}\right)^{1/2} {\rm cm},$$

about a factor of 3 smaller than the value inferred from measurement of the Hα peak separation.

A final possibility to consider is that decay is not truly exponential. While the exponential model provides an excellent fit to the data and is preferred by the AIC to a linear fit, the exponential model has four free parameters fit to seven data points. Moreover, plateaus, reflares, and other temporal discontinuities are well attested in the literature (e.g., Chen et al. 1997). As an ad hoc exploration, we fit a linear decay model to the first four data points of the X-ray flux light curve (Figure 5, gray dashed line), which yielded $\tau_l = 61.2 \pm 0.5$ days. Since the number of data points is small the fit is reasonable, leaving the last three points to be interpreted as a plateau. This scenario is admittedly finely tuned, however.

4. Discussion

Because XTE J1859+226 underwent a full outburst in 1999, we can be confident that the differences in the properties of this recent outburst are due to changes in the accretion process rather than in the fundamental system parameters. Using the peak separation of the Hα emission lines, we inferred the outer radius of the optically emitting disk. While our SED fits imply that the disk was locally hot enough to ionize hydrogen, the observed peak X-ray luminosity was insufficient to ionize the entire disk by two orders of magnitude. Surprisingly, the X-ray light curve showed an exponential decay characteristic of an ionized disk. This contradicts the expectation (Heinke et al. 2015) that faint outbursts from long-period XRBs will have exclusively linear declines. Several strands of evidence suggest that our estimate of the outer disk radius is too high by a factor of a few, but this is insufficient to resolve the discrepancy. Alternatively, the observed X-ray light curve could be interpreted as a linear decline followed by a plateau.

The peak X-ray flux in this outburst was two orders of magnitude too low to be detected by all-sky monitors such as MAXI and Swift-BAT. Thus without optical monitoring this outburst would have gone undetected. However, modern synoptic surveys such as ZTF, ATLAS (Tonry et al. 2018), ASAS-SN (Shappee et al. 2014), and Gattini-IR (De et al. 2020) scan most of the visible sky every few nights. When paired with an alerting system that can filter the millions of transient and variable sources they produce, these wide-field surveys can provide a powerful new approach to identifying X-ray binary outbursts despite being untargeted. While their temporal coverage of known XRBs depends on the survey's chosen footprint and cadence, synoptic surveys can provide excellent light curves, as this example illustrates (see Figures 1 and 2). Additionally, unlike targeted optical surveys of known XRBs, all-sky surveys can also discover brand new X-ray binaries (e.g., ASASSN-18ey/MAXI J1820+070, Tucker et al. 2018; AT2019wey, Yao et al. 2021), particularly those with short orbital periods (Tetarenko et al. 2016, and references therein). Because they are more sensitive than all-sky X-ray monitors, they provide an opportunity to identify outbursts early and to characterize samples of low-luminosity failed-transition outbursts (Wang et al. 2023). Thanks to its depth and Southern Hemisphere site, the upcoming Legacy Survey of Space and Time conducted by the Vera C. Rubin Observatory (Ivezić et al. 2019) will provide decade-long light curves for the majority of visible XRBs. These data will provide an unprecedented real-time view of XRBs in quiescence and enable rapid multiwavelength follow-up of outbursts.

Acknowledgments

Based on observations obtained with the Samuel Oschin Telescope 48 inch and the 60 inch Telescope at the Palomar Observatory as part of the Zwicky Transient Facility project. ZTF is supported by the National Science Foundation under grants No. AST-1440341 and AST-2034437 and a collaboration including current partners Caltech, IPAC, the Weizmann Institute of Science, the Oskar Klein Center at Stockholm University, the University of Maryland, Deutsches Elektronen-Synchrotron and Humboldt University, the TANGO Consortium of Taiwan, the University of Wisconsin at Milwaukee, Trinity College Dublin, Lawrence Livermore National Laboratories, IN2P3, University of Warwick, Ruhr University Bochum, Northwestern University and former partners the University of Washington, Los Alamos National Laboratories, and Lawrence Berkeley National Laboratories. Operations are conducted by COO, IPAC, and UW.

SED Machine is based upon work supported by the National Science Foundation under grant No. 1106171.

The ZTF forced photometry service was funded under the Heising–Simons Foundation grant #12540303 (PI: Graham).

This work made use of data supplied by the UK Swift Science Data Centre at the University of Leicester.

We acknowledge with thanks the variable star observations from the AAVSO International Database contributed by observers worldwide and used in this research.

This research has made use of a collection of ISIS functions (ISISscripts) provided by ECAP/Remeis observatory and MIT (http://www.sternwarte.uni-erlangen.de/isis/).

This research has made use of the MAXI data provided by RIKEN, JAXA and the MAXI team.

E.C.B., R.P., and Y.K. gratefully acknowledge support from the NSF AAG grant 1812779 and grant #2018-0908 from the Heising–Simons Foundation.

E.C.B. acknowledges further support from the Vera C. Rubin Observatory, which is supported in part by the National Science Foundation through Cooperative Agreement 1258333 managed by the Association of Universities for Research in Astronomy (AURA), and the Department of Energy under Contract No. DE-AC02-76SF00515 with the SLAC National Accelerator Laboratory. Additional LSST funding comes from private donations, grants to universities, and in-kind support from LSSTC Institutional Members. M.W.C. acknowledges support from the National Science Foundation with grant Nos. PHY-2010970 and OAC-2117997.

Facilities: PO:1.2m (Zwicky Transient Facility), PO:1.5m (SEDM), Keck:I (LRIS), Swift, AAVSO.

Software: `FPipe` (Fremling et al. 2016), `pysedm` (Rigault et al. 2019), `LPipe` (Perley 2019), `PySpecKit` (Ginsburg & Mirocha 2011; Ginsburg et al. 2022), ISIS (Houck & Denicola 2000), `astropy` (Astropy Collaboration et al. 2013; The Astropy Collaboration et al. 2018), `matplotlib` (Hunter 2007), `numpy` (Van Der Walt et al. 2011; Harris et al. 2020), `seaborn` (Waskom et al. 2018), `pandas` (McKinney 2010), `jupyter` (Kluyver et al. 2016), `ipython` (Pérez & Granger 2007).

ORCID iDs

Eric C. Bellm https://orcid.org/0000-0001-8018-5348
Yuankun Wang https://orcid.org/0000-0001-5538-0395
Jan van Roestel https://orcid.org/0000-0002-2626-2872
Rebecca A. Phillipson https://orcid.org/0000-0001-6891-7091
Michael W. Coughlin https://orcid.org/0000-0002-8262-2924
John A. Tomsick https://orcid.org/0000-0001-5506-9855
Steven L. Groom https://orcid.org/0000-0001-5668-3507
Brian Healy https://orcid.org/0000-0002-7718-7884
Josiah Purdum https://orcid.org/0000-0003-1227-3738
Ben Rusholme https://orcid.org/0000-0001-7648-4142
Jesper Sollerman https://orcid.org/0000-0003-1546-6615

References

Akaike, H. 1974, ITAC, 19, 716
Alabarta, K., Altamirano, D., Méndez, M., et al. 2021, MNRAS, 507, 5507
Arnaud, K. A. 2000, Parameter Estimation in X-ray Astronomy in the Chandra and XMM-Newton Era, https://heasarc.gsfc.nasa.gov/docs/xanadu/xspec/wstat.ps
Astropy Collaboration, Robitaille, T. P., Tollerud, E. J., et al. 2013, A&A, 558, A33
Baglio, M. C., Saikia, P., Russell, D. M., et al. 2022, ApJ, 930, 20
Bahramian, A., Heinke, C. O., Kennea, J. A., et al. 2021, MNRAS, 501, 2790
Bellm, E. C. 2021a, ATel, 14372, 1
Bellm, E. C. 2021b, ATel, 14375, 1
Bellm, E. C., Kulkarni, S. R., Barlow, T., et al. 2019a, PASP, 131, 068003
Bellm, E. C., Kulkarni, S. R., Graham, M. J., et al. 2019b, PASP, 131, 018002
Blagorodnova, N., Neill, J. D., Walters, R., et al. 2018, PASP, 130, 035003
Brocksopp, C., Fender, R. P., McCollough, M., et al. 2002, MNRAS, 331, 765
Caruso, E., Baglio, M. C., Saikia, P., et al. 2021, ATel, 14415, 1
Casares, J. 2016, ApJ, 822, 99
Chen, W., Shrader, C. R., & Livio, M. 1997, ApJ, 491, 312
Corral-Santana, J. M., Casares, J., Shahbaz, T., et al. 2011, MNRAS, 413, L15
Corral-Santana, J. M., Rodríguez-Gil, P., Hurley, D., & Casares, J. 2010, ATel, 2845, 1
Coughlin, M. W., Bloom, J. S., Nir, G., et al. 2023, ApJS, 267, 31
Cox, A. N. 2000, in Allen's Astrophysical Quantities, ed. A. Cox (New York: AIP Press)
dal Fiume, D., Frontera, F., Orlandini, M., et al. 1999, IAUC, 7291, 2
De, K., Hankins, M. J., Kasliwal, M. M., et al. 2020, PASP, 132, 025001
Dekany, R., Smith, R. M., Riddle, R., et al. 2020, PASP, 132, 038001
Draghis, P. A., Miller, J. M., Balakrishnan, M., et al. 2021, ATel, 14512, 1
Draghis, P. A., Miller, J. M., Zoghbi, A., et al. 2023, ApJ, 946, 19
Evans, P. A., Beardmore, A. P., Page, K. L., et al. 2007, A&A, 469, 379
Evans, P. A., Beardmore, A. P., Page, K. L., et al. 2009, MNRAS, 397, 1177
Farinelli, R., Amati, L., Shaposhnikov, N., et al. 2013, MNRAS, 428, 3295
Filippenko, A. V., & Chornock, R. 2001, IAUC, 7644, 2
Fitzpatrick, E. L. 1999, PASP, 111, 63
Focke, W. B., Markwardt, C. B., Swank, J. H., & Taam, R. E. 2000, Rossi2000: Astrophysics with the Rossi X-ray Timing Explorer, 104
Fremling, C., Sollerman, J., Taddia, F., et al. 2016, A&A, 593, A68
Garnavich, P. M., Stanek, K. Z., & Berlind, P. 1999, IAUC, 7276, 1
Ginsburg, A., Sokolov, V, de Val-Borro, M, et al. 2022, AJ, 163, 291
Ginsburg, A., Sokolov, V., de Val-Borro, M., et al. 2022, AJ, 163, 291
Graham, M. J., Kulkarni, S. R., Bellm, E. C., et al. 2019, PASP, 131, 078001
Hameury, J. M. 2020, AdSpR, 66, 1004
Harris, C. R., Millman, K. J., van der Walt, S. J., et al. 2020, Natur, 585, 357
Heinke, C. O., Bahramian, A., Degenaar, N., & Wijnands, R. 2015, MNRAS, 447, 3034
Houck, J. C., & Denicola, L. A. 2000, in ASP Conf. Ser. 216, Astronomical Data Analysis Software and Systems IX, ed. N. Manset, C. Veillet, & D. Crabtree (San Francisco, CA: ASP), 591
Hunter, J. D. 2007, CSE, 9, 90
Hynes, R. I. 2005, ApJ, 623, 1026
Ivezić, Ž., Kahn, S. M., Tyson, J. A., et al. 2019, ApJ, 873, 111
Kaastra, J. S., & Bleeker, J. A. M. 2016, A&A, 587, A151
Kalemci, E., Kara, E., & Tomsick, J. A. 2022, in Handbook of X-ray and Gamma-ray Astrophysics, ed. C. Bambi & A. Santangelo (Singapore: Springer Nature), 9
Kim, Y. L., Rigault, M., Neill, J. D., et al. 2022, PASP, 134, 024505
King, A. R., & Ritter, H. 1998, MNRAS, 293, L42
Kloppenborg, B. K. 2022, Observations from the AAVSO International Database, https://www.aavso.org
Kluyver, T., Ragan-Kelley, B., Pérez, F., et al. 2016, in Positioning and Power in Academic Publishing: Players, Agents and Agendas, ed. F. Loizides & B. Scmidt (Netherlands: IOS Press), 87, https://eprints.soton.ac.uk/403913/
Krimm, H. A., Holland, S. T., Corbet, R. H. D., et al. 2013, ApJS, 209, 14
Kuulkers, E., Shaw, S. E., Paizis, A., et al. 2007, A&A, 466, 595

Lasota, J. P., Dubus, G., & Kruk, K. 2008, A&A, 486, 523
Markwardt, C. B., Marshall, F. E., & Swank, J. H. 1999, IAUC, 7274, 2
Masci, F. J., Laher, R. R., Rusholme, B., et al. 2019, PASP, 131, 018003
Matheson, T., Stubens, C., Wolf, N., et al. 2021, AJ, 161, 107
Matsuoka, M., Kawasaki, K., Ueno, S., et al. 2009, PASJ, 61, 999
McKinney, W. 2010, in Proc. 9th Python in Science Conf., ed. S. van der Walt & J. Millman, 56
Oke, J. B., Cohen, J. G., Carr, M., et al. 1995, PASP, 107, 375
Patterson, M. T., Bellm, E. C., Rusholme, B., et al. 2019, PASP, 131, 018001
Pérez, F., & Granger, B. E. 2007, CSE, 9, 21
Perley, D. A. 2019, PASP, 131, 084503
Pooley, G. G., & Hjellming, R. M. 1999, IAUC, 7278, 1
Remillard, R. A., & McClintock, J. E. 2006, ARA&A, 44, 49
Rigault, M., Neill, J. D., Blagorodnova, N., et al. 2019, A&A, 627, A115
Russell, D. M., Bramich, D. M., Lewis, F., et al. 2019, AN, 340, 278
Saikia, P., Russell, D. M., Pirbhoy, S. F., et al. 2023, ApJ, 949, 104
Shahbaz, T., Charles, P. A., & King, A. R. 1998, MNRAS, 301, 382
Shappee, B. J., Prieto, J. L., Grupe, D., et al. 2014, ApJ, 788, 48
Swank, J., & Markwardt, C. 2001, in ASP Conf. Ser. 251, New Century of X-ray Astronomy, ed. H. Inoue & H. Kunieda (San Francisco, CA: ASP), 94
Tetarenko, B. E., Dubus, G., Lasota, J. P., Heinke, C. O., & Sivakoff, G. R. 2018a, MNRAS, 480, 2
Tetarenko, B. E., Lasota, J. P., Heinke, C. O., Dubus, G., & Sivakoff, G. R. 2018b, Natur, 554, 69
Tetarenko, B. E., Sivakoff, G. R., Heinke, C. O., & Gladstone, J. C. 2016, ApJS, 222, 15
The Astropy Collaboration, Price-Whelan, A. M., Sipőcz, B. M., et al. 2018, AJ, 156, 123
Tomsick, J. A., Corbel, S., Fender, R., et al. 2003, ApJL, 597, L133
Tonry, J. L., Denneau, L., Heinze, A. N., et al. 2018, PASP, 130, 064505
Tucker, M. A., Shappee, B. J., Holoien, T. W.-S., et al. 2018, ApJL, 867, L9
Van Der Walt, S., Colbert, S. C., & Varoquaux, G. 2011, CSE, 13, 22
van der Walt, S. J., Crellin-Quick, A., & Bloom, J. S. 2019, JOSS, 4, 1247
Verner, D. A., Ferland, G. J., Korista, K. T., & Yakovlev, D. G. 1996, ApJ, 465, 487
Wachter, K., Leach, R., & Kellogg, E. 1979, ApJ, 230, 274
Wagner, R. M., Smith, P. S., Schmidt, G. D., & Shrader, C. R. 1999, IAUC, 7279, 1
Wang, Y., Bellm, E., Crossland, A., et al. 2023, ApJ, submitted
Wijnands, R., in't Zand, J. J. M., Rupen, M., et al. 2006, A&A, 449, 1117
Waskom, M., Botvinnik, O., O'Kane, D., et al. 2018, Seaborn v0.9.0, Zenodo, doi:10.5281/zenodo.1313201
Willingale, R., Starling, R. L. C., Beardmore, A. P., Tanvir, N. R., & O'Brien, P. T. 2013, MNRAS, 431, 394
Wilms, J., Allen, A., & McCray, R. 2000, ApJ, 542, 914
Wood, A., Smith, D. A., Marshall, F. E., & Swank, J. 1999, IAUC, 7274, 1
Yao, Y., Kulkarni, S. R., Burdge, K. B., et al. 2021, ApJ, 920, 120
Zhang, G. B., Bernardini, F., Russell, D. M., et al. 2019, ApJ, 876, 5
Zurita, C., Sánchez-Fernández, C., Casares, J., et al. 2002, MNRAS, 334, 999